



OPEN

SUBJECT AREAS:
ELECTRONIC DEVICES
CONJUGATED POLYMERSReceived
31 July 2014Accepted
9 October 2014Published
29 October 2014Correspondence and
requests for materials
should be addressed to
S.-A.C. (sachen@che.
nthu.edu.tw)

Single Junction Inverted Polymer Solar Cell Reaching Power Conversion Efficiency 10.31% by Employing Dual-Doped Zinc Oxide Nano-Film as Cathode Interlayer

Sih-Hao Liao, Hong-Jyun Jhuo, Po-Nan Yeh, Yu-Shan Cheng, Yi-Lun Li, Yu-Hsuan Lee, Sunil Sharma & Show-An Chen

Chemical Engineering Department and Frontier Research Center on Fundamental and Applied Sciences of Matters, National Tsing-Hua University, No. 101, Section 2, Kuang-Fu Road, Hsinchu, Taiwan, 30013 (Republic of China).

We present high efficiency and stable inverted PSCs (i-PSC) by employing sol-gel processed simultaneously doped ZnO by Indium and fullerene derivative (BisNPC60-OH) (denoted as InZnO-BisC60) film as cathode interlayer and PTB7-Th:PC₇₁BM as the active layer (where PTB7-Th is a low bandgap polymer we proposed previously). This dual-doped ZnO, InZnO-BisC60, film shows dual and opposite gradient dopant concentration profiles, being rich in fullerene derivative at the cathode surface in contact with active layer and rich in In at the cathode surface in contact with the ITO surface. Such doping in ZnO not only gives improved surface conductivity by a factor of 270 (from 0.015 to 4.06 S cm⁻¹) but also provides enhanced electron mobility by a factor of 132 (from 8.25*10⁻⁵ to 1.09*10⁻² cm² V⁻¹ s⁻¹). The resulting i-PSC exhibits the improved PCE 10.31% relative to that with ZnO without doping 8.25%. This PCE 10.31% is the best result among the reported values so far for single junction PSC.

Bulk-heterojunction (BHJ) polymer solar cell (PSC)¹⁻³ with an active layer composed of a conjugated polymer as the donor and a fullerene derivative as the acceptor has attracted great attention because of its ease of fabrication, promising flexibility, and capability for large-scale and low-cost production. For conjugated polymer/fullerene BHJ solar cells, state of the art power conversion efficiencies (PCEs) of exceeding 9% (9.11%⁴, 9.21%⁵ and 9.35%⁶) for single junction cell, and up to 10.6%⁷ for tandem junction cell have been achieved.

To reach high PCE, one has to use low band gap polymer as donor with deep highest occupied molecular orbital (HOMO) energy level for harvesting more sunlight (and thus higher short circuit current (J_{sc})) and higher open circuit voltage (V_{oc}), and to use interlayer or electrode modification for effective collection of charges. Among the reported effective low band gap polymers, the series of copolymers composed of the two basic fused rings comonomer units, benzodithiophene (BDT) and thieno[3,4-b]thiophene (TT), are of particular interest since they offer high PCE (7-8%)⁸⁻¹³ resulting from high J_{sc} and V_{oc}.

For improvement in electron and hole collections for further PCE enhancement, insertions of interlayers between the active layer and the electrodes have been made. PEDOT:PSS is usually used as anode interlayer in conventional PSC (c-PSC). However, prolonged exposure of this kind of device to air can lead to an oxidation of the air sensitive metal cathode, resulting in a degradation of PSC¹⁴. In order to alleviate this problem, an approach involved an inversion of the device architecture (i-PSC) is employed, in which a less air-sensitive high work function metal (Ag, Au) is used as the back hole collecting electrode and ZnO (metal oxide) is used as the electron collecting interlayer between ITO and active layer¹⁵⁻¹⁷. The ZnO is an n-type material with wide band gap (3.3 eV)¹⁸, in which intrinsic defects such as excess zinc at the interstitial position and oxygen vacancy make ZnO n-type¹⁸. The conductivity of its thin film depends on temperature and atmosphere of thermal treatment^{19,20}. When doped with other dopants Al, In or Ga, the conductivity is enhanced by extrinsic defects and can be as high as 50 S cm⁻¹ for sol-gel processed indium doped ZnO¹⁸. Such Indium doped ZnO film also has high transparency

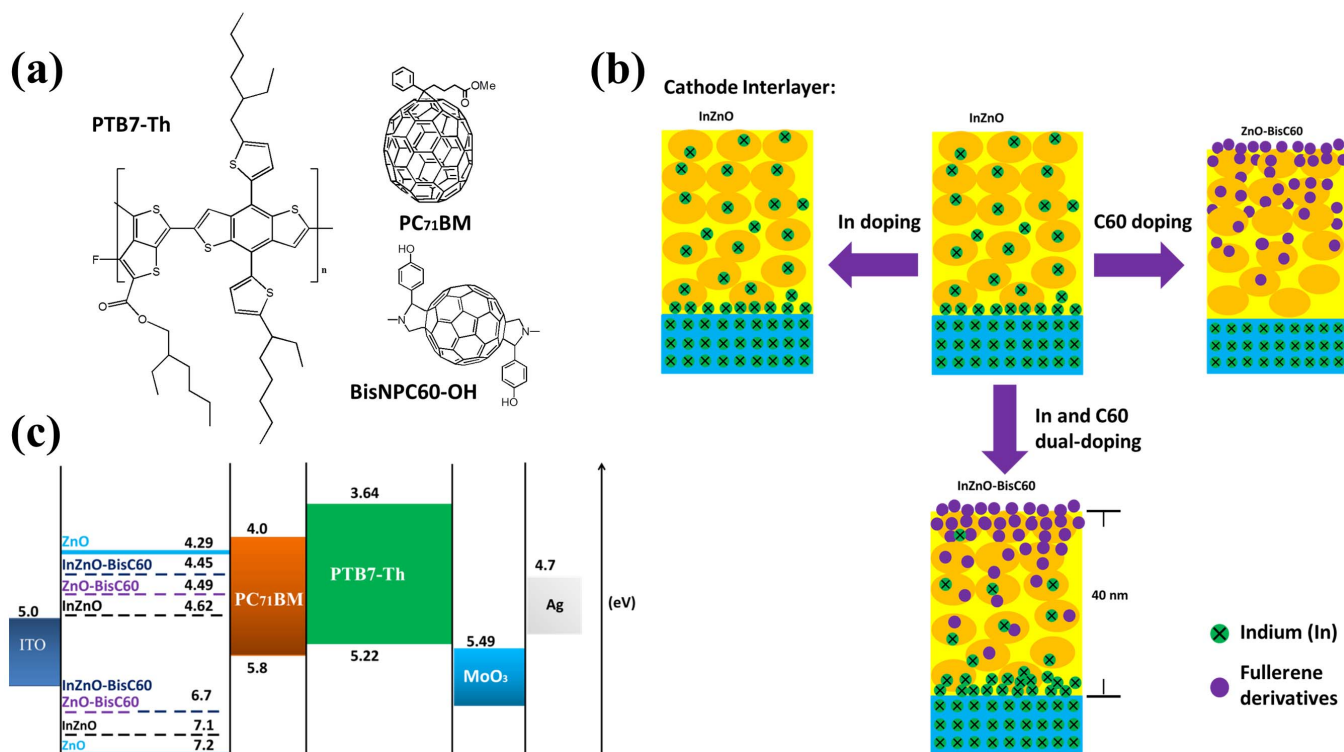


Figure 1 | (a) Chemical structures of the materials used for device fabrication; (b) Schematic illustration of the proposed cathode interlayer from XPS depth profile; (c) Energy levels diagram for ZnO, InZnO, ZnO-BisC60 and InZnO-BisC60 determined from UPS, and UV-vis results and for all the other materials taken from ref. 5 (for PTB7-Th, PC₇₁BM) ref. 40 (for MoO₃).

and can be used as transparent charge collecting electrode in solar cell. In i-PSC, it was reported that use of Mg doped ZnO thin film as the cathode buffer layer with an active layer PTB7:PC₇₁BM gave improvement in PCE from 7.11% to 8.35%²¹. However, the inorganic electron collecting electrode could have poor interfacial contact with organic active layer resulting in a poor electron extraction²² in i-PSC. Thus the cathode interface modification is a crucial issue for i-PSC, requiring high transparency, high electron mobility, and appropriate energy level for matching with lowest unoccupied molecular orbital (LUMO) level of acceptor.

In i-PSC, introducing cathode interlayer for improvement of PCE has been demonstrated, such as self-assembled monolayer (SAM) of fullerene derivatives^{23,24}, crosslinkable fullerene derivative²⁵, and polyelectrolytes²⁶. Recently, it was reported that the use of fullerene derivative (PCBE-OH) doped ZnO as the cathode for i-PSC with low band gap polymer PTB7-Th gave the PCE as high as 9.35%⁶. This cathode provides dual functionalities for enhanced electron collection, including producing a fullerene-derivative-rich cathode surface and high surface conductivity.

Here we report high efficiency and stable inverted PSCs (i-PSC) by employing sol-gel processed simultaneously doped ZnO by Indium and fullerene derivative (BisNPC60-OH) (denoted as InZnO-BisC60) film as cathode interlayer and PTB7-Th:PC₇₁BM as the active layer (where PTB7-Th is a low bandgap polymer we proposed previously⁶). This dual-doped ZnO, InZnO-BisC60, film shows dual and opposite gradient dopant concentration profiles, being rich in fullerene derivative at the cathode surface in contact with the active layer and rich in In at the cathode surface in contact with the ITO surface. Such doping in ZnO not only gives improved surface conductivity by a factor of 270 (from 0.015 to 4.06 S cm⁻¹) but also provides enhanced electron mobility by a factor of 132 (from 8.25*10⁻⁵ to 1.09*10⁻² cm² V⁻¹ s⁻¹). The resulting i-PSC exhibits the improved PCE 10.31% relative to that with ZnO without doping

8.25%. This PCE 10.31% is the best result among the reported values so far for single junction PSC.

Results

ZnO-BisC60 and ZnO nano-films (40 nm) were prepared by spin-casting from the solution of 1.5 wt% BisNPC60-OH and 98.5 wt% Zn(Ac)₂ (1g, total) and from the same solution but without BisNPC60-OH in the mixture of THF/2-methoxyethanol (1 : 4, v/v, 10 ml) and ethanolamine (0.252 g) on top of ITO and then sintering at 180°C, respectively. The InZnO and InZnO-BisC60 nano-films (40 nm) were also prepared in accordance with the above method but to the solutions, 1 atom% InCl₃ were added in addition. The procedure for preparation of ZnO-BisC60 nano-film is different from that in our previous report for ZnO-C60 nano-film⁶ since the structure of the fullerene derivatives used are different. Here the fullerene derivative used was based on bis-functional phenol group on C60 BisNPC60-OH (solubility = 1.5 mg/ml) (Fig. 1a) which has better solubility than that with functional alcohol group PCBE-OH (solubility = 0.5 mg/ml) both in the mixed solvent of THF/2-methoxyethanol (1 : 4, v/v). The resulting InZnO-BisC60, InZnO, ZnO-BisC60, and ZnO films on ITO were then rinsed with carbon disulfide (CS₂) and THF to remove the nonbonding residual BisNPC60-OH on the surface and subsequently dried for further characterization by contact angle measurement, X-ray and ultraviolet photoelectron spectroscopy (XPS and UPS), ultraviolet-visible absorption spectroscopy (UV-vis), and charge transport measurement. The details of UPS, XPS, and general instrumental measurements are described in the supplementary information.

The contact angles from the measurement with water drop as the probe for the surface of the cathode interlayers are shown in Fig. S1. The doping of BisNPC60-OH into InZnO and ZnO leads to improved hydrophobicity as reflected in the contact angle increasing from 30° to 67° and from 25° to 55°, respectively. Referring to the



contact angle of C60-SAM ranging from 40° to 60° ²³, it can be inferred that the surfaces of InZnO-BisC60 and ZnO-BisC60 are mostly covered with the fullerene derivative. We also prepared the samples of fullerene doped ZnO and InZnO as ETL coated on ITO glass for AFM morphology measurement as shown in Fig. S2. The surface roughness of ZnO and InZnO are 2.28 nm and 2.67 nm, respectively, and those of the fullerene doped films ZnO-BisC60 and InZnO-BisC60 films are 6.63 nm and 3.54 nm, respectively. These roughness results indicate that those with fullerene doping have significantly increased roughness, which also support that their surfaces are rich in fullerenes.

XPS measurement for binding energy (BE) spectra of various types of carbon on the surfaces of cathode interlayer nano-films are shown in Fig. 2a, in which each of ZnO and InZnO shows a major peak and a very weak peak, the former contributing from the carbons of C-O-R²⁷ for ZnO (285.2 eV) and for InZnO (285.2 eV), while the latter from the carbons of carbonyl group (288.9 eV)²⁷. When InZnO and ZnO are doped with the fullerene derivative (BisNPC60-OH), as expected, their intensities of C 1s BE peaks are both stronger than those without doping, since the fullerene derivative (BisNPC60-OH) is primarily composed of carbon atoms. The major C 1s peaks grow dramatically and shift to 285.6 eV (InZnO-BisC60) and 285.7 eV (ZnO-BisC60) contributing from the fullerene derivatives^{6,28,29} and the minor C 1s peaks (288.9 eV) are from the carbons of carbonyl group²⁷. The C 1s BE intensities for InZnO-BisC60 and ZnO-BisC60 are much stronger than those of our previous ZnO-C60 due to the better solubility of the fullerene derivative BisNPC60-OH (solubility = 1.5 mg/ml) in the THF/methoxyethanol (1:4, v/v) than that of PCBE-OH (solubility = 0.5 mg/ml) allowing more BisNPC60-OH (1.5 wt%) to be added than PCBE-OH (0.5 wt%).

Further analysis of XPS results on BE spectra for zinc, indium and oxygen atoms at the surfaces of the cathode interlayers shown in Fig. 2b, 2c and 2d are given below to reveal that ZnO in InZnO, ZnO-BisC60 and InZnO-BisC60 are doped either by indium or BisNPC60-OH or by both. As can be seen, the BE peaks of InZnO (Zn 2p_{1/2} (1022.7 eV) and 2p_{3/2} (1045.7 eV)), are both lower by 0.3 eV than those of ZnO (Zn 2p_{1/2} (1023.0 eV) and 2p_{3/2} (1046.0 eV)). In the cases of InZnO-BisC60 and ZnO-BisC60, both pairs of the BE peaks of the former (Zn 2p_{1/2} (1022.5 eV) and 2p_{3/2} (1045.5 eV)) and those of the latter (Zn 2p_{1/2} (1022.3 eV) and 2p_{3/2} (1045.3 eV)) are lower by 0.5 eV and 0.7 eV than those of ZnO, respectively. The indium spectra BE in Fig. 2c exhibit two significant peaks at 444.6 (In 3d_{3/2}) and 452.4 eV (In 3d_{5/2}) which can be attributed to In-O in In₂O₃ by shifting to higher energy by 0.7 eV relative to the pristine In (3d_{3/2} 443.9 eV)³⁰. The peak of In 3d_{5/2} peak at 444.9 eV contributed from InCl₃ was not observed³⁰, suggesting that dopant InCl₃ is completely decomposed during the sol-gel or annealing process. The BE peaks of O 1s in the ZnO are 532.5 eV and 531.2 eV for O-H³¹ and Zn-O³¹, respectively; while those in the InZnO also give two peak at 532.8 eV and 531.5, which can be attributed to O-H³¹ and Zn-O³¹ in ZnO by shifting to higher energy by 0.3 eV relative to the pristine ZnO. The peak of BE O 1s at 532.5 eV (OH) disappears in the ZnO-BisC60 and InZnO-BisC60, indicating that the defect with O-H on the ZnO surface is eliminated after the doping, which would also contribute partially to the enhancement in electron extraction efficiency³². Since the fullerene content in the total solid of the precursor is only 1.5 wt% and the surface is fullerene rich, it is necessary to examine the atom content profiles along the InZnO-BisC60 layer. It can be clearly observed from Fig. 2e that at the surface, C/Zn atom ratio of ZnO-C60 (0.98) is higher than that of ZnO (0.23) by 0.75 (or a factor of 4.13), which is also higher than that of unsintered homogeneous case (0.25) by a factor of 3 (because the C/Zn of unsintered InZnO-BisC60 is calculated to be 4.25 and that of ZnO is 4). This indicates that the surface of InZnO-BisC60 is rich in fullerene derivative. Whereas In/Zn atom ratio profile in InZnO-BisC60 cases is nearly zero before the

sputtering time at about 800s and appears a small increasing peak at sputtering time 900s in the range 800–1020s, which would indicate that the sputtering time 1020s is equivalent to the thickness of InZnO-BisC60 layers, 40 nm and the sputtering time from 800 to 1020s is mainly located within the dopant indium rich region. For the InZnO case, the depth profile of In/Zn would indicate that the sputtering time 1260s is equivalent to the thickness of InZnO layer, 40 nm; and the increase in In-content after 1260s is contributed from In in ITO layer in ITO glass. The C/Zn atom ratio profile of InZnO-BisC60 (0.98 at the surface) is reduced rapidly to 0.22 at the sputtering time 300s, indicating that the fullerene derivative in InZnO-BisC60 is mainly located within the interfacial region 11.8 nm (or 12 nm) as estimated by assuming a linear variation of sputtering time with thickness. Therefore the gradient distribution of fullerene content can be depicted as Fig. 1b. This InZnO-BisC60 manifests a new dual doping of zinc oxide nano-film (as interlayer with ITO cathode) by Indium and novel fullerene derivative, which results in a dual gradient concentration profiles with opposite distributions of the two dopants, being rich in fullerene derivative at the surface and rich in indium at the interface with the ITO cathode.

To investigate if ZnO in the bulk of InZnO, ZnO-BisC60, or InZnO-BisC60 is also doped by Indium, fullerene, or both, we examined their UV-vis spectra (Fig. S3a) before doping. The pristine film ZnO has absorption edge at about 400 nm, but after the dopings, the three doped ZnO shows additional absorption in the range 400 to 550 nm, indicating the occurrence of doping in the bulk by which additional electronic states are generated in the band gap^{6,33,34}. We then turn to determine the electronic energy levels (HOMO and LUMO levels of ZnO, InZnO, ZnO-BisC60 and InZnO-BisC60) using UPS (Fig. S3 and Table S1) (the detail measurement is described in supplementary information). The HOMO levels of ZnO-BisC60 and InZnO-BisC60 (6.7 eV and 6.7 eV) are lowered by 0.5 eV and 0.4 eV relative to those of ZnO and InZnO (7.20 eV and 7.1 eV). Note that such change is due to the n-doping rather than interfacial dipole as evidenced by the generation of additional optical absorption indicated above. The LUMO levels of ZnO, InZnO, ZnO-BisC60 and InZnO-BisC60 can then be determined by subtracting optical optical band gaps determined from the optical absorption spectra in Fig. S3a from the HOMO levels to give 2.91, 2.48, 2.21 and 2.25 eV, respectively. The resulting LUMO levels are 4.29 eV (ZnO), 4.62 eV (InZnO), 4.49 eV (ZnO-BisC60) and 4.45 eV (InZnO-BisC60). The doping creates a new transport pathway for electrons. The energy levels so determined along with those of the other materials are summarized in Fig. 1c.

In InZnO, ZnO-BisC60 and InZnO-BisC60, the created electronic states by doping would allow an improvement in conductivity relative to ZnO as expected. We measured electron mobility (μ) across these films by applying single carrier space charge limited conduction (SCLC) on the electron-only device, ITO/cathode interlayer/Ca/Al, and the results are shown in Fig. S4 and Table S2. All of the electron mobilities for these films are significantly higher than those without doping, and the electron mobility decreases in the sequence InZnO-BisC60 ($1.09 \times 10^{-2} \text{ cm}^2 \text{ V}^{-1} \text{ s}^{-1}$) > InZnO ($9.51 \times 10^{-3} \text{ cm}^2 \text{ V}^{-1} \text{ s}^{-1}$) > ZnO-BisC60 ($6.21 \times 10^{-3} \text{ cm}^2 \text{ V}^{-1} \text{ s}^{-1}$) > ZnO ($8.25 \times 10^{-5} \text{ cm}^2 \text{ V}^{-1} \text{ s}^{-1}$) (the value for ZnO is close to the reported value $8.4 \times 10^{-5} \text{ cm}^2 \text{ V}^{-1} \text{ s}^{-1}$ in the same device)²¹. In addition the InZnO-BisC60 shows the highest electron mobility among all the materials. Furthermore, we also measured the surface conductivities for all these materials using the four probe method and found that the surface conductivity increases in the sequence from 0.015 (ZnO) to 2.03 (ZnO-BisC60) to 4.06 (InZnO-BisC60) to 8.51 (InZnO) S cm⁻¹ (Table S3).

We then apply the doped ZnO films by spin-coating of their precursors on ITO and then subject to sintering at 180°C as the cathode interlayer for i-PSC with the device structure ITO/cathode interlayer/PTB7-Th: PC₇₁BM/MoO₃/Ag. The device performances were

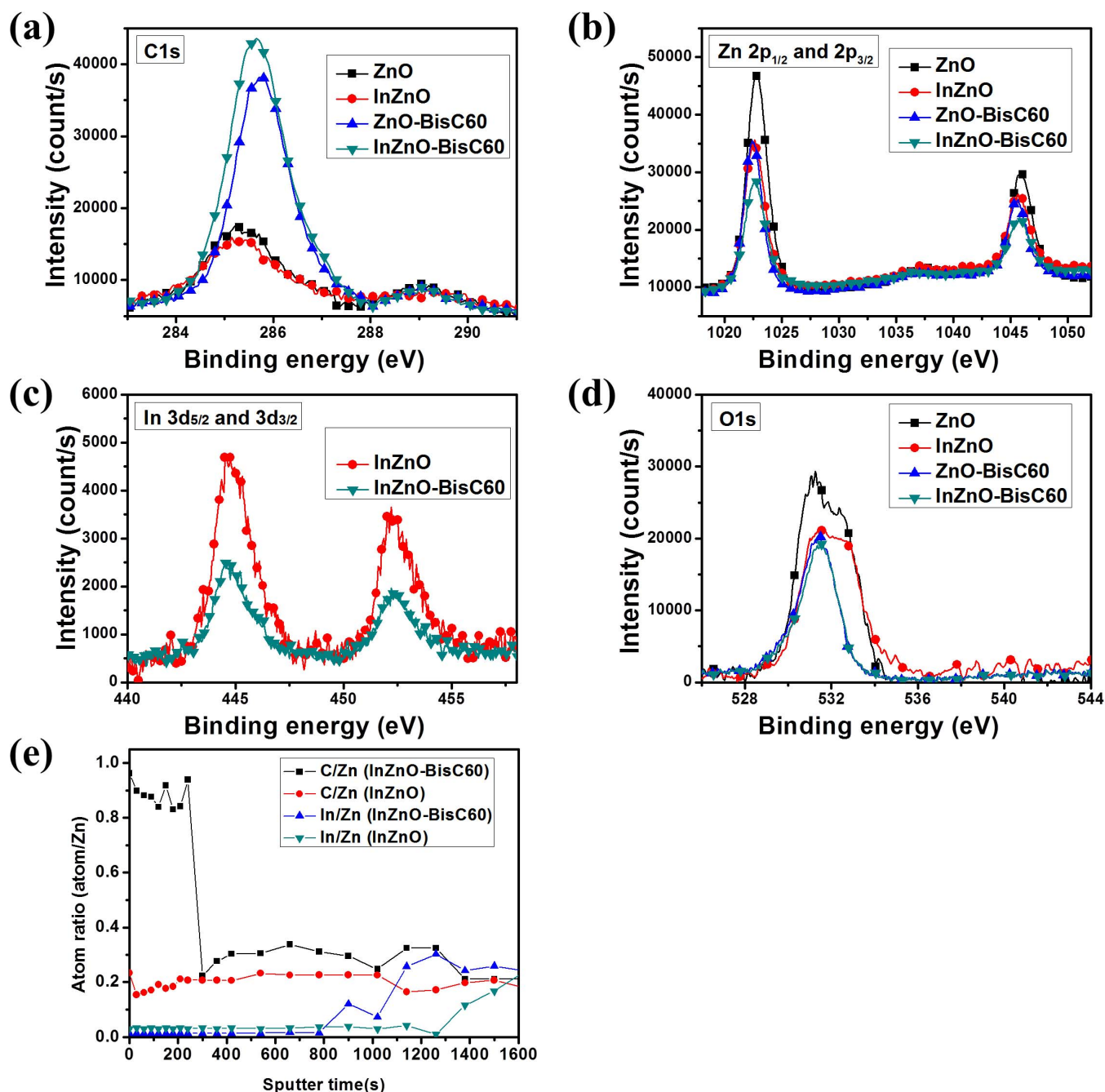


Figure 2 | XPS analysis on cathode interlayer: (a) carbon (285.2 eV (C1s)); (b) Zinc (1023.0 eV ($2p_{3/2}$) and 1046.0 eV ($2p_{1/2}$)); (c) Indium (444.6 eV ($2d_{5/2}$) and 452.4 eV ($2d_{3/2}$)); (d) Oxygen (531 eV (O 1s)) BE; and (e) depth profiles of the atom ratios C/Zn and In/Zn in InZnO and InZnO-BisC60.

measured under simulated 100 mW cm^{-2} AM 1.5G illumination as shown in Fig. 3a and their characteristic values are listed in Table 1. For the devices with doped ZnO's (including InZnO, ZnO-BisC60 and InZnO-BisC60), the PCE (maximum) enhances significantly from 8.25% (pristine ZnO) to 9.11% (InZnO), 9.71% (ZnO-BisC60) and to 10.31% (InZnO-BisC60). External quantum efficiency (EQE) measurements for the devices with InZnO-BisC60, ZnO-BisC60 and InZnO show overall enhancement in the entire absorption range (400 to 750 nm) when the doped cathodes are used to replace ZnO as the cathode interlayer (Fig. 3b), which implies that the increase of current density results from more efficient electron collection by doped ZnO's than ZnO. With BisNPC60-OH-doped interlayer InZnO-BisC60 and ZnO-BisC60, the EQEs from 500 to 700 nm and 375 to 500 nm of the former are in the range 68–80%

and 53–73%, and of the latter in 64–77% and 57–72%, which are much higher than those with InZnO 63–74% and 50–68%, with ZnO 58–69% and 46–61%, respectively. The additional electron collection enhancement can also be manifested by the calculations of series resistance (R_s) and shunt resistance (R_{sh}) from reciprocals of the slopes of the J-V curves at $I=0$ and $V=0$ ^{35–37}. For the devices with ZnO, InZnO, ZnO-BisC60 and InZnO-BisC60, these calculations show a significant drop in R_s from 10.12 to 4.56, 3.76 and 2.12 $\Omega \text{ cm}^2$, respectively, and a drastic rise in R_{sh} from 1120 to 1290, 1520 and 1610 $\Omega \text{ cm}^2$, respectively (Table S4). These indicate that the devices with fullerene or Indium doped cathode actually give a reduced R_s by promotion of electron transport at the interface and in the bulk of the cathode. In addition to charge transport, charge recombination also affects the charge collection efficiency³⁸. To

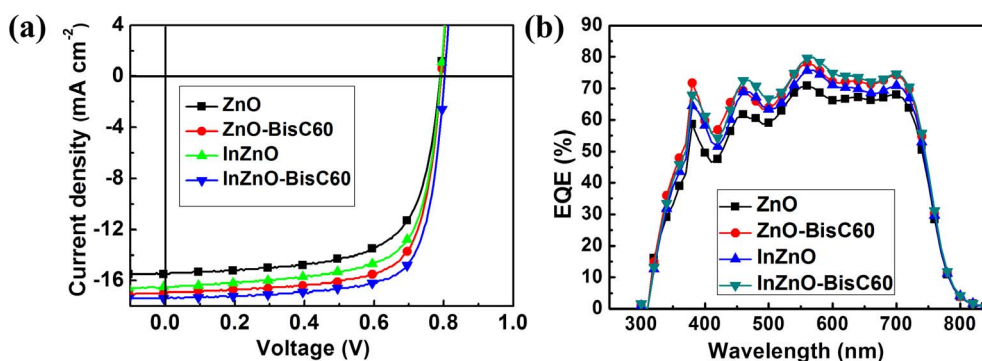


Figure 3 | Performance of i-PSC under simulated 100 mW cm^{-2} AM 1.5G illumination. (a) J-V curves of the devices ITO/cathode interlayer (40 nm)/PTB7-Th:PC₇₁BM (1 : 1.5 w/w, 100 nm)/MoO₃ (10 nm)/Ag (100 nm). (b) EQE spectra of the devices identical to those in (a).

investigate charge recombination, we measured the J-V curves of the devices (ITO/ZnO, InZnO or InZnO-BisC60/active layer/MoO₃/Ag) under various light intensity ranging from 100 mW/cm^2 to 4.32 mW/cm^2 and plotted J_{sc} versus illumination intensity (I) as shown in Fig. S5(a–c). The fitting of J_{sc} versus I with the power law relationship³⁹, $J_{sc} \propto I^\alpha$, where $\alpha (\leq 1)$ is ideality factor and is given in Fig. S5(d). This power law relationship describes the charge recombination kinetics at short circuit for BHJ PSC; as $\alpha = 1$, no recombination occurs, and deviation from 1 indicates an extent of charge recombination. For the ZnO, InZnO, InZnO-BisC60 devices, the α increases from 0.94 to 0.96, and to 0.98. InZnO-BisC60 has the highest α value 0.98, which implies that the extent of charge recombination is extremely low. This is correlated with the observed increase in Rsh and thus charge collection probability at short circuit. This decreased sequence in R_s and increased in Rsh of the devices with ZnO, InZnO and InZnO-BisC60 are in consistent with the promoted sequence of FF.

According to the characterization of InZnO-BisC60 and ZnO-BisC60 above, the improvement in PCE can be attributed mainly to the additional transport pathway for electrons created by the high coverage of the fullerene derivatives on InZnO and ZnO surface (Fig. 1b) and to the promoted electron conduction on surface and in the bulk of InZnO-BisC60 and ZnO-BisC60. Therefore the chance for electron/hole recombination at the interface is reduced by cutting off the chance of direct contact of polymer with ZnO or InZnO, facilitating a more effective collection of electrons from the bulk. The devices with InZnO-BisC60 (10.31%) and ZnO-BisC60 (9.71%) provide higher PCE than those without fullerene doping (InZnO and ZnO) by about 1.20% and 1.46%, respectively. Therefore the improvement in PCE from 8.25% (ZnO) to 10.31% (InZnO-BisC60) mainly results from the promotion of controllable fullerene distribution on the surface and bulk conductivity by dual functional doped species to provide dual functionality based on organic and inorganic compounds in the ZnO. Overall this work proposes dual functional doping of ZnO (one by fullerene derivative and the other by InCl₃ doping) for the device with the active layer PTB7-Th:PC₇₁BM, which lead to a great improvement in PCE from 8.25% to 10.31%.

Conclusion

In conclusion, we present a simple and novel method for modification of ZnO as the cathode interlayer for i-PSC by dual doping with the novel fullerene derivative (BisNPC60-OH) and indium (InCl₃) simultaneously. In this novel InZnO-BisC60 cathode interlayer, dual gradient concentration profiles with opposite distributions of the two dopants appear; the fullerene derivative-rich surface of this ZnO permits an improved electron collection by improved contacts with PC₇₁BM on the active layer surface and the In-rich ZnO bottom surface in contact with the ITO electrode permits an improved electron transport on surface and in bulk in this ZnO film. With this InZnO-BisC60 as the cathode interlayer, the device with the active layer PTB7-Th:PC₇₁BM gives the PCE 10.31% higher than that of ZnO without doping 8.25% by about 2%. The PCE of 10.31% is the best results that have been reported so far for single junction PSC.

Methods

PTB7-Th was from ONE material; [6,6]-phenyl C₇₁ butyric acid methyl ester (PC₇₁BM) was from Nano-C (99.5% purity), chlorobenzene (CB) from J. T. Baker (99.0% purity), and 1,8-dioctane from Sigma-Aldrich (98.0% purity).

Synthesis of C60-Substituted bis-Phenol (BisNPC60-OH). BisNPC60-OH was synthesized by the procedure similar to the published procedure²³, but the reaction temperature and purification steps are different. 4-hydroxybenzaldehyde (0.5 g, 3.5 mmol) and N-methylglycine were dissolved in 120 mL of chlorobenzene in a dried three-necked reaction flask with a magnetic stirring bar and a thermometer under N₂ purging condition at 110°C. C60 (0.5 g, 0.7 mmol) was added to the stirred solution at room temperature. The reaction was carried out under refluxing temperature at 135°C with continuously stirring for 1 day. The mixture was cooled down to room temperature and transferred to rotary evaporator for concentrating it to 5–10 mL at about 0.1 torr. After the residue was washed with methanol for several times, and then redissolved in the solvent (THF: Toluene, 1 : 1, v/v), the resulting solution was concentrated in a rotary evaporator and then reabsorbed on silica gel. Finally, the desired compound was purified by silica gel column chromatography with toluene as eluent and then precipitated by acetone. Finally, it was collected by filtration and dried in vacuum oven at 80°C for more than 20 hr. Total 115 mg BisNPC60-OH desired compound (yield: 16.1%) was obtained. Structure analysis of BisNPC60-OH: ¹HNMR (500 MHz, CS₂:CDCl₃). δ (ppm): 7.62–7.55 (d, 4H), 6.83–6.78 (d, 4H), 4.85 (s, 4H), 4.75 (broad, 2H), 4.24 (s, 2H), 2.15 (s, 6H). FAB MS calculated C₇₈H₂₂O₂N₂; m/z = 1018. Found: m/z = 1018.

i-PSC fabrication. For i-PSC, thin film of ZnO was prepared similar to the previously published procedures³¹, in which ZnO precursor solution was spin-cast at 5000 rpm

Table 1 | Photovoltaic performance of i-PSC based on PC₇₁BM with the device structure ITO/Cathode interlayer (40 nm)/PTB7-Th:PC₇₁BM (1 : 1.5 w/w, 100 nm)/MoO₃ (10 nm)/Ag (100 nm). (Each parameter is an average of five devices)

Cathode interlayer	Jsc [mA cm ⁻²]	Voc [V]	FF [%]	PCE (average) [%]	PCE (maximum) [%]
ZnO	15.32 ± 0.15	0.79 ± 0.005	67.1 ± 0.4	8.12 ± 0.13	8.25
ZnO-BisC60	16.88 ± 0.12	0.79 ± 0.005	72.0 ± 0.3	9.60 ± 0.11	9.71
InZnO	16.32 ± 0.10	0.79 ± 0.005	70.0 ± 0.2	9.03 ± 0.08	9.11
InZnO-BisC60	17.24 ± 0.05	0.80 ± 0.005	74.1 ± 0.4	10.22 ± 0.09	10.31



on top of a cleaned ITO, and then sintered at 180 °C for 1 hr in air, resulting in transparent ZnO thin film with the thickness about 40 nm. The ZnO precursor solution was prepared by dissolving zinc acetate dihydrate ($C_4H_6O_4Zn \cdot 2(H_2O)$ 99.5% from Merck, 1 g) and monoethanolamine ($HOCH_2CH_2NH_2$, 98% from Acros, 0.252 g) in 2-methoxyethanol (10 ml) under stirring for 8 hr for hydrolysis reaction and aging. The InZnO precursor solution was prepared by dissolving zinc acetate dihydrate (991.5 mg), Indium (III) chloride ($InCl_3$, 99.99% from Alfa Aesar, 9.85 mg, 1% mole ratio) and monoethanolamine in 2-methoxyethanol (10 ml) stirring for 8 hr for hydrolysis reaction and aging. And InZnO-BisC60 and ZnO-BisC60 precursor was prepared by dissolving zinc acetate dihydrate (975.15 mg), $InCl_3$ (9.85 mg, 1% mole ratio), BisNPC60-OH (15 mg), monoethanolamine and that without $InCl_3$ in THF/2-methoxyethanol (1 : 4, v/v, 10 ml) stirring for 8 hr for hydrolysis reaction and aging. On top of ZnO, InZnO, ZnO-BisC60, and InZnO-BisC60 film, a thin layer (about 100 nm) PTB7-Th:PC₇₁BM (1 : 1.5, w/w) was spin-cast from its solution in chlorobenzene/1,8-diiiodoethane (97 : 3, v/v) in argon-filled glove box. All the procedures were carried out in a glove box with argon, except those for ITO cleaning, and precursor spin coating for ZnO, InZnO, ZnO-BisC60, and InZnO-BisC60. Finally, a thin layer of MoO₃ (about 10 nm) covered with a layer of Ag (100 nm) as the anode were deposited successively in a vacuum thermal evaporator through a shadow mask at a pressure of less than 2×10^{-6} torr. The active area of the device is about 6 mm².

J-V characterization and EQE measurement. The current-voltage (J-V) characteristics of the unencapsulated PSCs were measured in air using a Keithley 2400 source-measure unit and an AM 1.5G solar simulator (Oriol 94021A, 150 W from Newport). The illumination intensity of 100 mW cm⁻² irradiation was calibrated using a KG5-filtered NREL-traceable monocrystal Si reference cell to ensure the accurate light source intensity. The external quantum efficiency (EQE) was conducted using the measurement system (model QE-R) built by Enli Technology Co. Ltd. Same data acquisition system was used for the external quantum efficiency measurement. Under full computer control, light from a 150 W xenon lamp (Oriol, U.S.A.) was focused through a monochromator onto the PSC under testing. The wavelength of the light from the monochromator was increased progressively in the visible region to generate the EQE (λ) as defined by $EQE(\lambda) = 1240 (J_{sc}/\lambda\phi)$, where λ is the wavelength in nm, J_{sc} is short-circuit photocurrent density (mA cm⁻²), and ϕ is the incident radiative flux (mW cm⁻²). J-V characteristics and EQE of the unencapsulated PSCs were measured in air.

General measurements and characterization. ¹HNMR spectra were recorded on a VARIAN UNITYINOVA 500 NMR in the NSC Regional Instrument Centre at National Tsing Hua University, Taiwan. FAB Mass spectra were also collected using MICROMASS TRIO-2000 in the NSC Regional Instrument Centre at National Chiao Tung University, Taiwan. The thickness of the active layer film, hole transport layer, cathode interlayer film were measured by a Tencor P-10 Surface Profiler. Contact angle with water was measured using contact angle meter (GBX DIGIDROP). UV-vis spectra was measured using an UV-vis spectrometer (Perkin-Elmer, Lambda 19). The conductivity was measured by the four point probe method (Swin, SN: 3S100-0901). Electron mobility of the interlayers (ZnO, InZnO, ZnO-BisC60 and InZnO-BisC60) determined using the electron only device ITO/cathode interlayer/Ca/Al along with the use of single carrier space charge limited current (SCLC) equation for the calculation. The current density from SCLC follows the Mott-Gurney Law by the equation³⁶: $9\epsilon_0\epsilon_r\mu(V-V_{bi})^2/8L^3$, where ϵ_0 is the permittivity of free space, ϵ_r is the dielectric constant of the materials, μ is the carrier mobility, V is the applied voltage across device, V_{bi} is the built-in voltage, and L is the thickness of the film. For X-ray photoelectron spectroscopy (XPS) measurements, the ZnO, InZnO, ZnO-BisC60 and InZnO-BisC60 film were obtained from their precursors on top of ITO glasses sintered at air at 180 °C for 60 min (the same as those described above for device fabrication). XPS spectra were obtained with a photoelectron spectroscopy system (VG, MULTILAB 2000) under a base pressure of 1×10^{-9} mbar by using monochromatized Mg (K α) X-rays ($h\nu = 1254.6$ eV). During depth profiling, sputter erosion was performed using a raster scanned Ar⁺ ion beam of 2 keV primary energy at an angle of incidence of 45° with a current density of 2 μ A cm⁻².

Ultraviolet Photoelectron Spectroscopy. We used the ultraviolet photoelectron spectroscopy (UPS, from Thermo Electron Corporation) to study the surface electronic energy levels of cathode interlayer as shown in Fig. S3b. The HOMO level of InZnO-BisC60 and ZnO-BisC60 are 6.7 eV and 6.7 eV which are lower than those of InZnO (7.1 eV) and ZnO (7.2 eV) by 0.4 eV and 0.5 eV (Table S1). The HOMO level was determined by the following equation, HOMO level = $h\nu - (E_{cutoff} - E_{onset})$, where $h\nu$ is incident photon energy (21.2 eV) of He I, the high binding energy cutoff (E_{cutoff}) and HOMO region (E_{onset}) are the turning points shown in Fig. S1b. The E_{cutoff} was determined by linear extrapolation to zero at the yield of secondary electrons, and the E_{onset} is the onset relative to the Fermi level (E_f) of Au (0 eV), where the E_f is determined from the Au substrate. The LUMO level of cathode interlayer can then be determined by adding up their optical band gaps as follows: LUMO level = HOMO level-optical band gap, where optical band gap of ZnO, InZnO, ZnO-BisC60 and InZnO-BisC60 are 2.91, 2.48 eV, 2.21 eV, 2.25 eV, respectively. The LUMO levels are 4.29 (ZnO), 4.62 (InZnO), 4.49 (ZnO-BisC60) and 4.45 eV (InZnO-BisC60).

- Yu, G. *et al.* Polymer Photovoltaic Cells: Enhanced Efficiencies via a Network of Internal Donor-Acceptor Heterojunctions. *Science* **270**, 1789–1791 (1995).
- Ma, W. *et al.* Thermally Stable, Efficient Polymer Solar Cells with Nanoscale Control of the Interpenetrating Network Morphology. *Adv. Funct. Mater.* **15**, 1617–1622 (2005).
- Li, Y. *et al.* Molecular Design of Photovoltaic Materials for Polymer Solar Cells: Toward Suitable Electronic Energy Levels and Broad Absorption. *Acc. Chem. Res.* **45**, 723–733 (2012).
- Liu, S. *et al.* High-Efficiency Polymer Solar Cells via the Incorporation of an Amino-Functionalized Conjugated Metallopolymer as a Cathode Interlayer. *J. Am. Chem. Soc.* **135**, 15326–15329 (2013).
- He, Z. *et al.* Enhanced power-conversion efficiency in polymer solar cells using an inverted device structure. *Nat. Photonics* **6**, 591–595 (2012).
- Liao, S.-H. *et al.* Fullerene Derivative-Doped Zinc Oxide Nanofilm as the Cathode of Inverted Polymer Solar Cells with Low-Bandgap Polymer (PTB7-Th) for High Performance. *Adv. Mater.* **25**, 4766–4771 (2013).
- You, J. *et al.* A polymer tandem solar cell with 10.6% power conversion efficiency. *Nat. Commun.* **4**, 1446–1455 (2013).
- Chen, H. Y. *et al.* Polymer solar cells with enhanced open-circuit voltage and efficiency. *Nat. Photonics* **3**, 649–653 (2009).
- Liang, Y. *et al.* For the Bright Future—Bulk Heterojunction Polymer Solar Cells with Power Conversion Efficiency of 7.4%. *Adv. Mater.* **22**, 1–4 (2010).
- Huo, L. J. *et al.* Replacing Alkoxy Groups with Alkylthienyl Groups: A Feasible Approach To Improve the Properties of Photovoltaic Polymers. *Angew. Chem. Int. Ed.* **50**, 9697–9702 (2011).
- Zhang, M. *et al.* Synergistic Effect of Fluorination on Molecular Energy Level Modulation in Highly Efficient Photovoltaic Polymers. *Adv. Mater.* **26**, 1118–1123 (2014).
- Wu, Y. *et al.* PDT-S-T: A New Polymer with Optimized Molecular Conformation for Controlled Aggregation and π - π Stacking and Its Application in Efficient Photovoltaic Devices. *Adv. Mater.* **25**, 3449–3455 (2013).
- Kim, J. H. *et al.* Thieno[3,2-b]thiophene-Substituted Benzo[1,2-b:4,5 b']dithiophene as a Promising Building Block for Low Bandgap Semiconducting Polymers for High-Performance Single and Tandem Organic Photovoltaic Cells. *Chem. Mater.* **26**, 1234–1242 (2014).
- Krebs, F. C. *et al.* Analysis of the Failure Mechanism for a Stable Organic Photovoltaic During 10000 h of Testing. *Progr. Photovolt.: Res. Appl.* **15**, 697–712 (2007).
- Li, G. *et al.* Efficient inverted polymer solar cells. *Appl. Phys. Lett.* **88**, 253503 (2006).
- Hau, S. K. *et al.* Air-stable inverted flexible polymer solar cells using zinc oxide nanoparticles as an electron selective layer. *Appl. Phys. Lett.* **92**, 253301 (2008).
- Hau, S. K. *et al.* Interfacial modification to improve inverted polymer solar cells. *J. Mater. Chem.* **18**, 5113–5119 (2008).
- Kyaw, A. K. K. *et al.* The properties of sol-gel processed indium-doped zinc oxide semiconductor film and its application in organic solar cells. *Phys. Status Solidi A* **208**, 2635–2642 (2011).
- Goncalves, G. *et al.* Influence of post-annealing temperature on the properties exhibited by ITO, IZO and GZO thin films. *Thin Solid Films* **515**, 8562–8566 (2007).
- Barquinha, P. *et al.* Effect of annealing temperature on the properties of IZO films and IZO based transparent TFTs. *Thin Solid Films* **515**, 8450–8454 (2007).
- Yin, Z. *et al.* Graphene-Based Materials for Solar Cell Applications. *Adv. Energy Mater.* **4**, 1300574 (2014).
- Hsieh, C. H. *et al.* Highly Efficient and Stable Inverted Polymer Solar Cells Integrated with a Cross-Linked Fullerene Material as an Interlayer. *J. Am. Chem. Soc.* **132**, 4887–4893 (2010).
- Hau, S. K. *et al.* Effect of Chemical Modification of Fullerene-Based Self-Assembled Monolayers on the Performance of Inverted Polymer Solar Cells. *ACS Appl. Mater. Interfaces.* **2**, 1892–1902 (2010).
- Ma, D. *et al.* Self-Organization of Amine-Based Cathode Interfacial Materials in Inverted Polymer Solar Cells. *ACS Nano* **8**, 1601–1608 (2014).
- Cheng, Y.-J. *et al.* Combination of Indene-C60 Bis-Adduct and Cross-Linked Fullerene Interlayer Leading to Highly Efficient Inverted Polymer Solar Cells. *J. Am. Chem. Soc.* **132**, 17381–17383 (2010).
- Yang, T. *et al.* Inverted polymer solar cells with 8.4% efficiency by conjugated polyelectrolyte. *Energy Environ. Sci.* **5**, 8208–8214 (2012).
- Tan, S. T. *et al.* p-type conduction in unintentional carbon-doped ZnO thin films. *Appl. Phys. Lett.* **91**, 72101–3 (2007).
- Maxwell, A. J. *et al.* Photoemission, autoionization, anti x-ray-absorption spectroscopy of ultrathin-film C60 on Au(110). *Phys. Rev. B* **49**, 10717–10720 (1994).
- Felicissimo, M. P. *et al.* Determination of vertical phase separation in a polyfluorene copolymer:fullerene derivative solar cell blend by X-ray photoelectron spectroscopy. *J. Mater. Chem.* **19**, 4899–4901 (2009).
- Lee, D. Y. *et al.* Etch characteristics of indium zinc oxide thin films using inductively coupled plasma of a Cl₂/Ar gas. *Thin Solid Films* **517**, 4047–4051 (2009).
- Yang, B. *et al.* Structural and optical properties of N-doped ZnO nanorod arrays. *J. Phys. D: Appl. Phys.* **42**, 195402–5 (2009).



32. Sun, Y. *et al.* Inverted Polymer Solar Cells Integrated with a Low- Temperature-Annealed Sol-Gel-Derived ZnO Film as an Electron Transport Layer. *Adv. Mater.* **23**, 1679–1683 (2011).
33. Game, O. *et al.* Concurrent synthetic control of dopant (nitrogen) and defect complexes to realize broadband (UV–650 nm) absorption in ZnO nanorods for superior photo-electrochemical performance. *J. Mater. Chem.* **22**, 17302–17310 (2012).
34. Park, S.-M. *et al.* Structure and properties of transparent conductive doped ZnO films by pulsed laser deposition. *Appl. Surf. Sci.* **253**, 1522–1527 (2006).
35. Cheng, Y.-S. *et al.* Physically adsorbed fullerene layer on positively charged sites on zinc oxide cathode affords efficiency enhancement in inverted polymer solar cell. *ACS Appl. Mater. Interfaces* **5**, 6665–6671 (2013).
36. Moliton, A. *et al.* Review How to model the behaviour of organic photovoltaic cells. *Polym Int.* **55**, 583–600 (2006).
37. Liao, S.-H. *et al.* Multiple Functionalities of Polyfluorene Grafted with Metal Ion-Intercalated Crown Ether as an Electron Transport Layer for Bulk-Heterojunction Polymer Solar Cells: Optical Interference, Hole Blocking, Interfacial Dipole, and Electron Conduction. *J. Am. Chem. Soc.* **134**, 14271–14274 (2012).
38. Kong, J. *et al.* Top-Down Approach for Nanophase Reconstruction in Bulk Heterojunction Solar Cells. *Adv. Mater.* **26**, 6275–6283 (2014).
39. Gupta, V. *et al.* Barium: An Efficient Cathode Layer for Bulk-heterojunction Solar Cells. *Sci. Rep.*, DOI: 10.1038/srep01965 (2013).
40. Liu, J. *et al.* High-Efficiency Inverted Polymer Solar Cells with Transparent and Work-Function Tunable MoO₃-Al Composite Film as Cathode Buffer Layer. *Adv. Mater.* **24**, 2774–2779 (2012).

Acknowledgments

We thank Ministry of Education and the Ministry of Science and Technology for the financial aid through project NSC-101-2120-M-007-004, NSC-102-2633-M-007-002 and NSC 102-2221-E-007-131.

Author contributions

S.-H.L., H.-J.J. and S.-A.C. developed the idea. S.-H.L. and S.-A.C. designed the experiments, analyzed the data and wrote up the manuscript. S.-H.L. carried out the device fabrication and measurements. Y.-S.C., Y.-L.Li. and Y.-H.L. carried out XPS measurements and data analysis. P.-N.Y. and S.S. carried out synthesis of materials and characterizations.

Additional information

Supplementary information accompanies this paper at <http://www.nature.com/scientificreports>

Competing financial interests: The authors declare no competing financial interests.

How to cite this article: Liao, S.-H. *et al.* Single Junction Inverted Polymer Solar Cell Reaching Power Conversion Efficiency 10.31% by Employing Dual-Doped Zinc Oxide Nano-Film as Cathode Interlayer. *Sci. Rep.* **4**, 6813; DOI:10.1038/srep06813 (2014).



This work is licensed under a Creative Commons Attribution-NonCommercial-NoDerivs 4.0 International License. The images or other third party material in this article are included in the article's Creative Commons license, unless indicated otherwise in the credit line; if the material is not included under the Creative Commons license, users will need to obtain permission from the license holder in order to reproduce the material. To view a copy of this license, visit <http://creativecommons.org/licenses/by-nc-nd/4.0/>